Test Evaluation Method for Second-order Intermodulation False Alarm Interference

Xue DU, Guanghui WEI, Dalin WU, Xiaodong PAN

Shijiazhuang Campus of Army Engineering University, 97 Heping West Road, 050003, Shijiazhuang, Hebei, China

duxue_xdd@163.com, wei-guanghui@sohu.com, dalinwu@163.com, panxiaodong1980@sina.com

Submitted January 4, 2024 / Accepted April 17, 2024 / Online first May 13, 2024

Abstract. *Aiming at the quantitative evaluation requirements of radar second-order intermodulation false alarm (SIFA) effect, a radar SIFA effect model is established from the field-circuit coupling mechanism, and the parameter test method of the model is given. Taking a certain type of radar as the test object, the SIFA effect test is carried out by using the method of electromagnetic injection equivalent substitution irradiation. The results show that the tested radar will produce a SIFA signal higher than the selected sensitive level when the frequency difference of dual-frequency electromagnetic interference (EMI) is within 3 MHz and the frequency offset is within ±200 MHz. Using the model parameters of the SIFA interference effect measured in the experiment, it is assumed that they do not change with the interference field strength. Combined with the SIFA interference field strength of the tested radar and the single frequency blocking critical interference field strength, the effect model can evaluate the degree of radar SIFA interference.*

Keywords

Electromagnetic interference (EMI), second-order intermodulation false alarm (SIFA), radar, parameter test method of effect model

1. Introduction

With the development of science and technology, and the widespread use of electronic information equipment, the battlefield electromagnetic environment has become increasingly complex. Whether the frequency equipment has good adaptability to the electromagnetic environment has become an important guarantee of battlefield intelligence reconnaissance, joint command and control [1]. Radar equipment has been widely used in military and civil fields with its advantages of the all-weather and real-time acquisition of target information [2]. Currently, more and more scientists and research laboratories are conducting research on the electromagnetic environmental effects of frequency equipment. However, the widespread use of high-power frequency equipment has reduced radar detection performance. Therefore, the prediction of the multi-frequency electromagnetic interference (EMI) model for radar equipment has become one of the hot spots of research at home and abroad [3]. Liu et al discussed the effects of common noise and continuous waves (CW) on radar equipment and studied them in modeling and simulation without considering the influence of intermodulation components due to device nonlinearity [4]. References [5], [6] analyzed the adverse effects of out-of-band EMI on radar, but none of them involved the multi-frequency electromagnetic radiation intermodulation components. At present, many scholars have analyzed and studied third-order intermodulation, including mechanism analysis, model prediction, and special algorithms for avoiding third-order intermodulation interference [7–9]. References [10–12] pointed out that the second-order intermodulation signal is caused by nonlinear devices such as mixers and amplifiers in low-frequency circuits, and the mechanism of second-order intermodulation interference generation and determination methods have seldom been studied. References [13–16] analyzed the out-of-band multi-frequency non-intermodulation and third-order intermodulation blocking effects of communication radios and navigation receivers, and established the corresponding intermodulation blocking interference effect model of frequency equipment such as navigation and radio based on the single-frequency blocking effect. Traditionally, most scholars believe that second-order intermodulation signals are far away from the operating frequency band and do not cause significant interference, and there are relatively few studies on second-order intermodulation. Reference [17] reveals the second-order intermodulation blocking interference mechanism of navigation receivers from the inside of receivers. In response to the demand for experimental evaluation, reference [18] establishes a second-order intermodulation blocking model from the second-order intermodulation blocking mechanism by introducing the blocking interference factor, and the accuracy of the model is within 2 dB, but this model is not applicable to the second-order intermodulation false alarm jamming signal with radar. Due to the frequency of the radar receiver having a certain bandwidth, which will cause the false signal to be received incorrectly to form false alarm interference. Reference [19] analyzed the interference mechanism, wave-

DOI: 10.13164/re.2024.0329

form characteristics, and position variation of radar single-frequency, dual-frequency non-intermodulation, and SIFA signals, and the SIFA sensitive range and interference effect model are not mentioned. Based on this, aiming at the quantitative evaluation demand of radar second-order intermodulation false alarm effect, this paper establishes the second-order intermodulation false alarm effect model based on previous interference mechanism research and puts forward the parameter test method of radar second-order intermodulation false alarm model.

In this paper, in view of the quantitative evaluation requirements of the radar SIFA effect, based on the preliminary interference mechanism research, the SIFA effect model is established and the SIFA effect model parameter test method is proposed. Taking a certain type of radar as the equipment under test (EUT) to carry out the SIFA effect test. Firstly, the sensitive band of dual-frequency false alarm interference of the tested radar is preliminarily explored. Secondly, according to the parameter test method, the parameters of the SIFA model are obtained, and by changing the interference frequency difference and interference frequency offset, the correctness of the SIFA mechanism and the accuracy of the effect model are verified. It provides theoretical and technical support for the scientific evaluation of the adaptability of radar equipment to complex electromagnetic environments.

2. Second-order Intermodulation False Alarm Interference Effect Model

2.1 Establishing a Theoretical Model

The radar receives the target echo signal, which is mixed, amplified, and filtered by the RF front-end processing. When the device is subjected to a dual-frequency EMI signal close to the working frequency, due to the nonlinear distortion of the device, the interference signal generates an intermodulation signal through the second-stage mixer, and if the difference between the dual-frequency intermodulation frequency difference and the low-pass filter bandwidth of the level mixer is small, the second-order intermodulation signal can pass the filter and form a SIFA interference. In the imaging process of the SIFA target, there is only a single linear phase effect and no other phase effects. The energy of the SIFA signal is more concentrated, resulting in a single position fixed 'spike' false alarm target [19].

If the working center frequency of the EUT is f_0, the EMI field intensities at different frequencies in space are $E_i(f_i)$, $H_i(f_i)$ and $D_i(f_i)$ represent the transfer function from the electromagnetic field $E_i(f_i)$ to the RF front-end and the specific nonlinear device, respectively; the receiving equivalent level of RF front-end and the specific nonlinear device are expressed as $S_i(f_i)$ and $T_i(f_i)$ as follows:

$$S_i(f_i) = H_i(f_i)E_i(f_i), \tag{1}$$

$$T_i(f_i) = D_i(f_i)E_i(f_i) \tag{2}$$

where $i = 0$ means the same frequency signal as the EUT, $i \neq 0$ means a non-identical frequency signal. Due to the different frequencies of the signal, the antenna gain and circuit gain of the frequency equipment change, in addition to the circuit gain may also be related to f_0, so $H_i(f_i)$ and $D_i(f_i)$ are related to f_i and f_0.

Without loss of generality, set the SIFA signal generated be listed in the following equation:

$$\varphi_{F2}(\delta f) = KT_1(f_1)T_2(f_2) \tag{3}$$

where K is the SIFA nonlinear coefficient of EUT, and the intermodulation difference $\delta f = |f_1 - f_2|$. The above SIFA signal is easy to enter the low-frequency signal processing circuit. If the signal amplitude is large enough and is used as a useful signal processing, the tested radar may have a SIFA signal.

Set the SIFA interference threshold of the tested radar as $X(f)$, define the SIFA effect index as R_F, which can be expressed by the following equation:

$$R_F(\Delta f) = \frac{KT_1(f_1)T_2(f_2)}{X(\delta f)} \tag{4}$$

where $\Delta f_i = f_i - f_0$, from (4), it can be known that the SIFA interference occurs when $R_F \geq 1$, and the SIFA interference does not occur when the tested radar is $R_F < 1$.

In general, the single-frequency EMI sensitive port of the EUT is different from the SIFA sensitive port. From the previous analysis of radar EMI, it is known that the second-order intermodulation blocking signal is not obvious due to the stuttering phenomenon [19], while the SIFA shows a certain regularity. Secondly, under the existing conditions in the laboratory, the tested radar can get the complete single-frequency critical blocking interference sensitivity threshold, but not the single-frequency critical false alarm interference sensitivity threshold [20], based on this, the single-frequency blocking critical sensitivity threshold is used. Assuming that the single-frequency critical blocking EMI level and field strength corresponding to f_0 are C_0 and $E_{i0}(f_i)$, respectively, C_0 is only related to f_0, and the change factors related to the interference frequency f_i are included in the sensitivity coefficient $B_i(f_i)$, obtained [15]:

$$H_1B_1E_{10} = H_2B_2E_{20} = ... = H_0B_0E_{00} = C_0. \tag{5}$$

Substitute formulas (1) and (2) into (4), using (5) to get:

$$R_F(\Delta f) = \frac{C_0^2KD_1(f_1)D_2(f_2)}{X(\delta f)H_1(f_1)H_2(f_2)B_1(f_1)B_2(f_2)} \cdot \frac{E_1(f_1)E_2(f_2)}{E_{10}(f_1)E_{20}(f_2)}. \tag{6}$$

Let the relative value of the SIFA interference level is $X_r(\delta f) = X(\delta f) / X_{min}$, the SIFA interference coefficient is $\gamma = C_0D_i\sqrt{K / X_{min}} / (H_iB_i)$. In engineering, it is generally believed that $\gamma \approx \gamma(f_i - f_0)$, and the SIFA effect index R_F can be expressed as:

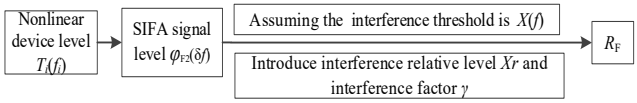

Fig. 1. Model derivation process flowchart.

$$R_{\mathrm{F}}(\delta f)=\frac{\gamma(\Delta f_1)\gamma(\Delta f_2)}{X_{\mathrm{r}}(\delta f)}\cdot\frac{E_1}{E_{10}}(f_1)\frac{E_2}{E_{20}}(f_2) \tag{7}$$

where E_1 and E_2 are the interference field strength when the interference signal f_1 and f_2 act together, and E_{10} and E_{20} are the single-frequency critical blocking interference field strengths corresponding to the interference signal f_1 and f_2 respectively.

For the convenience of understanding, the derivation process of the model is presented in the form of a flowchart in Fig. 1.

2.2 Parameter Solving

Let $R_{\mathrm{F}}=1$, take dB as a unit, and take the logarithm of both sides of (7) to obtain:

$$\gamma(\Delta f_1)+\gamma(\Delta f_2)+\frac{E_1}{E_{10}}(f_1)+\frac{E_2}{E_{20}}(f_2)=X_{\mathrm{r}}(\delta f) \tag{8}$$

where f_1 and f_2 interference field strength and their respective role in the single-frequency critical blocking interference field strength from the test measurement data to determine, and the other three covariates can be solved by associating multiple sets of experimental data.

Reference [15] describes the solution method of model parameters when the difference between the sensitive frequency offset and the sensitive frequency difference of frequency equipment such as navigation receiver was small, that is, four test frequency points are selected at equal frequency intervals to solve the model parameter, the equation is as follows:

$$\begin{cases}
\gamma(\Delta f_1)=\dfrac{1}{2}\left\{X_{\mathrm{r}}(2\tau)-\left[\dfrac{E_1}{E_{10}}+\dfrac{E_2}{E_{20}}\right]_{12}+\left[\dfrac{E_1}{E_{10}}+\dfrac{E_2}{E_{20}}\right]_{23}-\left[\dfrac{E_1}{E_{10}}+\dfrac{E_2}{E_{20}}\right]_{13}\right\},\\
\gamma(\Delta f_2)=\dfrac{1}{2}\left\{X_{\mathrm{r}}(2\tau)-\left[\dfrac{E_1}{E_{10}}+\dfrac{E_2}{E_{20}}\right]_{23}+\left[\dfrac{E_1}{E_{10}}+\dfrac{E_2}{E_{20}}\right]_{34}-\left[\dfrac{E_1}{E_{10}}+\dfrac{E_2}{E_{20}}\right]_{24}\right\},\\
\gamma(\Delta f_3)=\dfrac{1}{2}\left\{X_{\mathrm{r}}(2\tau)+\left[\dfrac{E_1}{E_{10}}+\dfrac{E_2}{E_{20}}\right]_{12}-\left[\dfrac{E_1}{E_{10}}+\dfrac{E_2}{E_{20}}\right]_{23}-\left[\dfrac{E_1}{E_{10}}+\dfrac{E_2}{E_{20}}\right]_{13}\right\},\\
\gamma(\Delta f_4)=\dfrac{1}{2}\left\{X_{\mathrm{r}}(2\tau)+\left[\dfrac{E_1}{E_{10}}+\dfrac{E_2}{E_{20}}\right]_{23}-\left[\dfrac{E_1}{E_{10}}+\dfrac{E_2}{E_{20}}\right]_{34}-\left[\dfrac{E_1}{E_{10}}+\dfrac{E_2}{E_{20}}\right]_{24}\right\},\\
X_{\mathrm{r}}(\tau)=X_{\mathrm{r}}(2\tau)+\\
\quad\dfrac{1}{2}\left\{\left[\dfrac{E_1}{E_{10}}+\dfrac{E_2}{E_{20}}\right]_{12}+\left[\dfrac{E_1}{E_{10}}+\dfrac{E_2}{E_{20}}\right]_{34}-\left[\dfrac{E_1}{E_{10}}+\dfrac{E_2}{E_{20}}\right]_{13}-\left[\dfrac{E_1}{E_{10}}+\dfrac{E_2}{E_{20}}\right]_{24}\right\},\\
X_{\mathrm{r}}(3\tau)=X_{\mathrm{r}}(2\tau)+\\
\quad\left[\dfrac{E_1}{E_{10}}+\dfrac{E_2}{E_{20}}\right]_{14}+\left[\dfrac{E_1}{E_{10}}+\dfrac{E_2}{E_{20}}\right]_{23}-\dfrac{1}{2}\left\{\left[\dfrac{E_1}{E_{10}}+\dfrac{E_2}{E_{20}}\right]_{12}+\left[\dfrac{E_1}{E_{10}}+\dfrac{E_2}{E_{20}}\right]_{13}\right.\\
\quad\left.-\left[\dfrac{E_1}{E_{10}}+\dfrac{E_2}{E_{20}}\right]_{24}-\left[\dfrac{E_1}{E_{10}}+\dfrac{E_2}{E_{20}}\right]_{34}\right\}.
\end{cases} \tag{9}$$

However, for radar equipment, the working sensitive frequency difference and the sensitive frequency deviation differ greatly, that is, $\delta f << \Delta f_i$, although the basic frequency extrapolation method has a comprehensive response, it will greatly increase the workload and calculation. Therefore, the sensitive frequency difference in the range of smaller changes can be considered $\gamma(\Delta f_1)\approx\gamma(\Delta f_2)$, formula (8) is simplified as follows:

$$\gamma(\Delta f_i)=\frac{1}{2}X_{\mathrm{r}}(\delta f)-\frac{1}{2}\left[\frac{E_1}{E_{10}}+\frac{E_2}{E_{20}}\right]. \tag{10}$$

Select two interference frequency points f_1 and f_2 to carry out the SIFA critical interference test, and the relationship $\gamma(\Delta f_i)$ with Δf_i and $X_{\mathrm{r}}(\delta f)$ with δf are determined. The specific method is as follows.

1) Adjust the interference frequency offset Δf_i. The SIFA critical interference test is carried out at different interference frequency offset Δf_1, $\Delta f_2=\Delta f_1+\tau$. Use (10) to determine the relationship between frequency offset interference coefficient $\gamma(\Delta f_i)$ and different interference frequency offsets Δf_i.

2) Adjust the interference frequency difference δf and carry out multiple groups of the SIFA critical interference test. Substitute the determined frequency offset interference coefficient into (10) to calculate the relationship between the relative value $[X_{\mathrm{r}}(\delta f)-X_{\mathrm{r}}(\tau)]$ and the δf, keep unknown $X_{\mathrm{r}}(\tau)$. Let the minimum value of $X_{\mathrm{r}}(\tau)$ is 0 dB, and determine the values of $X_{\mathrm{r}}(\delta f)$, $\gamma(\Delta f_i)$.

3. Second-order Intermodulation False Alarm Effect Test

The test method is the same as the radar dual-frequency EMI test method, the difference lies in the analysis of the second-order intermodulation waveform characteristics, position, level change law, and mechanism in the previous research [20], [21]. Based on the mechanism analysis, this paper takes the absolute level of SIFA as the index of the SIFA effect. The block diagram of the test is shown in Fig. 2. The test radar is a type of stepped-frequency ranging radar, working frequency is $f_0\pm 100$ MHz (f_0 is the center frequency). The EMI system consists of signal generators, power amplifier, directional coupler, combiner, and spectrum analyzer. Adjust the position of the target antenna so that it is in the sensitive direction of the EUT. According to GJB8848-2016 [22], adjust the output power and output frequency of the two signal generators to create the required electromagnetic environment, and the interference signals are transmitted to the EUT through the injection module.

Radar dual-frequency EMI signal imaging is shown in Fig. 3, where two "hill-shaped" electromagnetic signals for the dual-frequency non-intermodulation false alarm target, the waveform approximate "spike" type electromagnetic signal is a SIFA target with concentrated energy [19].

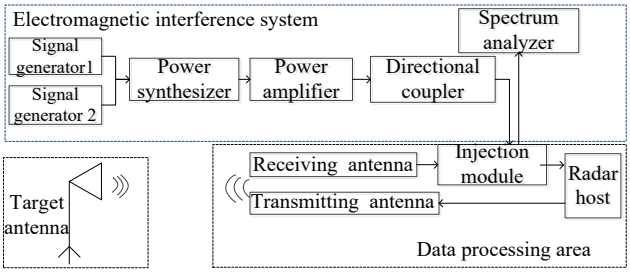

Fig. 2. The block diagram of SIFA interference test.

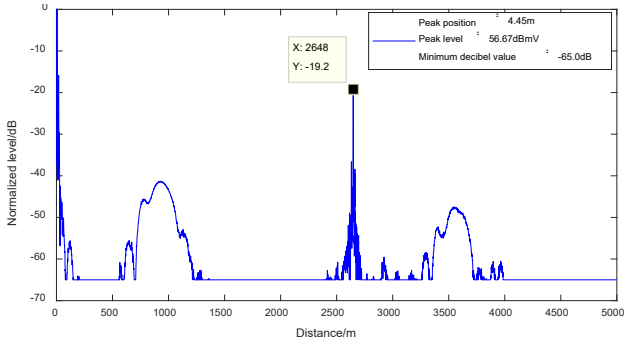

Fig. 3. SIFA interference imaging of EUT.

3.1 Second-order Intermodulation False Alarm Signal Stability Test and Calibration

The good repeatability and stability of the system itself is the necessary premise to ensure the equipment carries dual-frequency EMI test. The objective records ten SIFA signal data, and the system stability is improved by removing one maximum and minimum value and taking the average value for ten collected data. Select $E_1 = E_2$, $\Delta f_1 = 0$ Hz, $\Delta f_2 = 300$ kHz, adjust the signal source output power to increase in the same proportion, and record the SIFA signal level, the results are shown in Tab. 1.

According to Tab. 1, when the interference signal is small, the fluctuation range of SIFA is large, and the data stability is not good. The reason for this phenomenon is that when the interference signal is relatively small, the

E_1E_2 [dB(V/m)^2]	–20.0	–10.0	0.0	10.0	20.0
Serial number	**SIFA signal φ_{F2} [dBmV]**				
1	1.0	9.4	21.8	31.8	34.1
2	–1.9	9.4	19.6	29.3	35.4
3	0.0	10.3	19.6	31.6	35.2
4	–0.8	11	21.5	30.3	35.5
5	0.9	8.8	20.6	28.5	34.5
6	–1.9	9.5	20.5	31.0	33.6
7	–3.1	9.6	21.6	31.5	35.3
8	1.4	9.4	20.2	29.2	34.4
9	–0.7	9.6	19.9	30.1	33.1
10	–2.0	10.0	20.5	31.2	34.7
Average value	–0.7	9.7	20.6	30.5	34.7

Tab. 1. Test data of SIFA level with interference field strength.

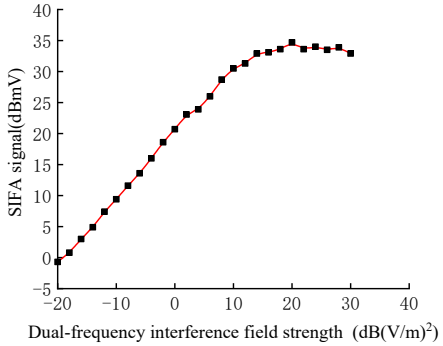

Fig. 4. Curve of SIFA signal with interference field strength.

dual-frequency non-intermodulation level is greater than the SIFA level. Combined with (3), if the sensitivity level is small, the accuracy of the calculated effect parameters is low, and the error is relatively large. The source of error is not theory but the instability of experimental data. The complete SIFA signal level is expressed as a function of the interference field strength, and the result is shown in Fig. 4.

It can be seen from Fig. 4 that: 1) When the dual frequency interference field strength is between-20 dB(V/m)^2 and 10 dB(V/m)^2, the SIFA signal level increases linearly with the increase of interference power. As the further increase of interference, the SIFA level growth rate decreases. 2) The SIFA sensitivity test is carried out after the sensitivity level is determined. To improve accuracy, select SIFA sensitivity as large as possible. This paper selects 10 dBmV as the SIFA sensitive level, and the experiment can also be carried out according to the practical application scenario. The sensitivity level can also be selected according to the actual situation, the test method is the same.

3.2 Preliminary Study on Second-order Intermodulation False Alarm Sensitive Band

Adjust the output power of the signal generator to make the double interference field strength to 10 dB(V/m)^2, set the dual-frequency interference frequency $f_1 = 0$ Hz, f_2 starts from 100 kHz and increased with 200 kHz, record the generated SIFA level, and the results are shown in Fig. 5.

It can be seen from Fig. 5 that with the increase of interference frequency difference δf, the SIFA level gradually decreases. When the interference frequency difference is greater than 2800 kHz, the SIFA signal is less than 5 dBmV. When the δf is greater than 3000 kHz, there is no obvious SIFA signal. Analysis of the reason is that when the δf is greater than a certain degree, the SIFA signal component falls outside the passband of the low-pass filter, and there will be no cause for SIFA interference. Similarly, the interference frequency offset $\Delta f_1 = 0$ Hz, the Δf_2 begins at 20 MHz and increases at 20 MHz, recording the SIFA signal level, and the results are shown in Fig. 6.

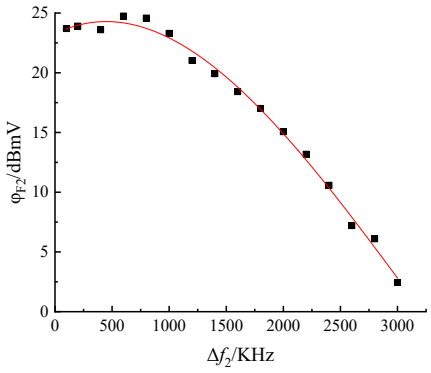

Fig. 5. The change curve of the SIFA level.

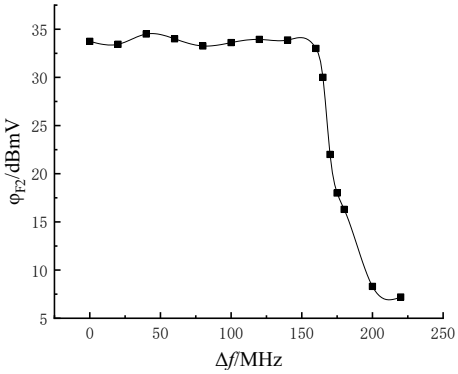

Fig. 6. Frequency bias range preliminary judgment.

It can be seen from Fig. 6 that when the interference frequency difference is greater than 160 MHz, the SIFA signal decreases sharply with the increase of interference frequency offset. It indicates that when the interference frequency difference is greater to a certain extent, the SIFA signal component falls outside the passband of the low-pass filter.

According to (5) and (7), it is necessary to know the single frequency critical blocking interference field strength $E_{i0}(f_i)$ of the tested radar. According to GJB 151B-2013 [23], select useful signal compression 6 dB as the single frequency blocking sensitive criterion, using the sensitivity test method to obtain the single frequency blocking sensitivity of the EUT, the result is shown in Fig. 7. It shows that the single frequency blocking and

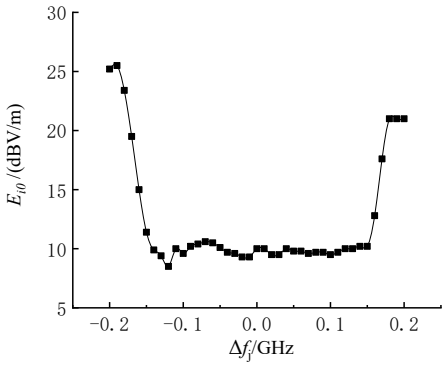

Fig. 7. Single frequency blocking sensitive threshold curve.

false alarm sensitive band range is about ±200 MHz, the phenomenon is mainly related to the filter bandwidth setting after the mixer of the radar RF front-end.

4. Effect Model Parameter Test

4.1 Feasibility Verification of the Test Method

According to Sec. 3, the sensitive frequency difference of the SIFA interference signal is about 3000 kHz, and the sensitive frequency offset is about 200 MHz. Four basic test points are selected according to the equal frequency interval τ of (9), and the two pairs are combined to conduct the SIFA interference test. And the SIFA frequency offset interference coefficient $\gamma(\Delta f_i)$ corresponding to each basic frequency point is calculated to determine the accuracy and feasibility of the approximate method.

Combined with Fig. 7, the single frequency interference field strength can be approximated within a small sensitive frequency difference range, that is $E_{10} \approx E_{20}$. To facilitate the calculation in dB, $E_1/E_{10}(f_1)$ $E_2/E_{20}(f_2)$ in (7) can be viewed as a whole. Set the frequency interval τ to be 200 kHz and 400 kHz, respectively. To distinguish between the two interference field strengths, E_1 and E_2 as far as possible to differ by more than 3 dB, select four base frequency points to be combined with each other for the SIFA critical interference test, and record the test data, as shown in Tab. 2 and Tab. 3.

Substituting the data in Tab. 2 into (9), the results are shown in Tab. 3.

It can be seen from Tab. 3 that when the frequency interval is 200 kHz and 400 kHz the interference coefficient $\gamma(\Delta f_i) - 0.5X_r(2\delta)$ error is within 1 dB, indicating that the EUT can be considered as $\gamma(\Delta f_1) \approx \gamma(\Delta f_2)$ when the sensitive frequency difference is small relative to the sensitive

Δf_1 [kHz]	0	200	400	0	200	0
Δf_2 [kHz]	200	400	600	400	600	600
E_1/E_{10}·E_2/E_{20} [dB]	–39.0	–39.3	–39.5	–39.4	–38.7	–38.8
Δf_1 [kHz]	0	400	800	0	400	0
Δf_2 [kHz]	400	800	1200	800	1200	1200
E_1/E_{10}·E_2/E_{20} [dB]	–39.0	–39.5	–38.9	–39.4	–39.5	–37.2

Tab. 2. Test data of SIFA under different interference frequency difference.

Δf_i [kHz]	0	200	400	600
$\lvert\gamma(\Delta f_i) - 0.5X_r(400)\rvert$ [dB]	19.6	19.2	19.8	19.5
Δf_1 [kHz]	0	400	800	1200
$\lvert\gamma(\Delta f_i) - 0.5X_r(800)\rvert$ [dB]	19.5	20.1	20.0	19.5

Tab. 3. Result of $\gamma(\Delta f_i)$ under different interference frequency difference.

frequency bias. In engineering processing, the approximation method of (10) can be used to simplify the calculation process.

4.2 Test to Determine the SIFA Effect Model Parameters [$\gamma(\Delta f_i) - 0.5X_r(2\tau)$]

Set $\tau = 200$ kHz, $\Delta f_1 = 0$ MHz, $\Delta f_2 = \Delta f_1 + \tau$, and the interference frequency offset increases with 20 MHz, and the test data of the SIFA critical interference field strength under different interference frequency offsets are obtained. When the change of interference field strength between the two frequency points is greater than 3 dB to take the interpolation point processing, the effect model parameters $\gamma(\Delta f_i) - 0.5X_r(\tau)$ under different interference frequency offsets are obtained by using (10). The calculation results are shown in Tab. 4.

It can be seen from Tab. 4 that when the interference frequency offset is in the range of 0~160 MHz, $[\gamma(\Delta f_i) - 0.5X_r(\tau)]$ remains almost constant. And relative interference frequency offset, within the small sensitive frequency deviation range of 3 MHz, the corresponding coefficients $[\gamma(\Delta f_i) - 0.5X_r(\tau)]$ at different frequencies are approximately equal.

4.3 Determination of Relative Low Frequency Interference Level $X_r(\delta f)$

In the sensitive frequency offset range, multiple frequency combinations with different frequency differences are selected to test the SIFA critical interference effect. Let $\Delta f_1 = 0$ kHz, Δf_2 starts at 100 kHz and increases at 100 kHz. Based on the test results of $[\gamma(\Delta f_i) - 0.5X_r(\tau)]$ obtained from Fig. 6, the relatively low-frequency interference levels under different interference frequency differences are calculated by (10). The results are shown in Tab. 5.

According to Tab. 5, let $X_r(\delta f)$ be a minimum of 0 dB, that is, $X_r(300)$ is 0 dB. The final value $X_r(\tau)$ is obtained, and the results are shown in Fig. 8.

It can be seen from Fig. 8 that $X_r(\delta f)$ of the SIFA signal shows a trend of 'first stable and then rising' with δf. The most sensitive frequency difference range of SIFA is about 1000 kHz. The difference between maximum and minimum $X_r(\delta f)$ is about 23 dB.

4.4 Test to Determine the SIFA Interference Coefficient $\gamma(\Delta f_i)$

By substituting $X_r(200)$ is 0.2 into Tab. 6 to obtain the $\gamma(\Delta f_i)$, the calculation results are shown in Tab. 6.

According to the mechanism of the SIFA effect, it is known that whether the interference frequency is higher or lower than the working frequency of the EUT, the relationship between $X_r(\delta f)$ and δf should be the same in theory. The next test is to determine $\gamma(\Delta f_i)$ and negative frequency offset. The same method is used to obtain negative frequency offset test results as shown in Fig. 9.

Comparing Fig. 9 and Tab. 6 get that the variation law of frequency offset coefficient $\gamma(\Delta f_i)$ with positive and negative frequency offsets is the same. And the reason is that the left and right frequency offsets of the EUT are the same due to the single-frequency blocking and the single-frequency false alarm critical interference sensitive band. Combined with the definition of the SIFA interference coefficient, it is speculated that $\gamma(\Delta f_i)$ is the same as the change law of negative frequency offset. The theoretical and

Δf_i [MHz]	0	20	40	60	80
$[\gamma(\Delta f_i) - 0.5X_r(2\tau)]$ [dB]	17.1	16.5	16.9	16.6	16.8
Δf_i [MHz]	100	120	140	160	165
$[\gamma(\Delta f_i) - 0.5X_r(2\tau)]$ [dB]	16.6	16.9	17.1	16.2	15.9
Δf_i [MHz]	170	175	180	200	220
$[\gamma(\Delta f_i) - 0.5X_r(2\tau)]$ [dB]	15.6	13.2	12.9	10.7	9.5

Tab. 4. Test result of $[\gamma(\Delta f_i) - 0.5X_r(\tau)]$.

$\Delta f = f_2 - f_1$ [kHz]	100	200	300	400	500
$[X_r(\delta f) - X_r(\tau)]$ [dB]	–4.1	–4.1	–4.3	–3.9	–3.8
$\Delta f = f_2 - f_1$ [kHz]	600	700	800	900	1000
$[X_r(\delta f) - X_r(\tau)]$ [dB]	–4.0	–4.1	–4.3	–4.1	–4.1
$\Delta f = f_2 - f_1$ [kHz]	1100	1200	1300	1400	1500
$[X_r(\delta f) - X_r(\tau)]$ [dB]	–3.0	–1.9	–0.1	–0.2	1.1
$\Delta f = f_2 - f_1$ [kHz]	1600	1700	1800	1900	2000
$[X_r(\delta f) - X_r(\tau)]$ [dB]	2.0	3.7	4.9	5.0	5.7
$\Delta f = f_2 - f_1$ [kHz]	2100	2200	2300	2400	2500
$[X_r(\delta f) - X_r(\tau)]$ [dB]	7.3	8.4	9.5	10.3	12.2
$\Delta f = f_2 - f_1$ [kHz]	2600	2700	2800	2900	3000
$[X_r(\delta f) - X_r(\tau)]$ [dB]	13.3	13.4	14.7	17.3	18.7

Tab. 5. Calculation result of $[X_r(\delta f) - X_r(\tau)]$.

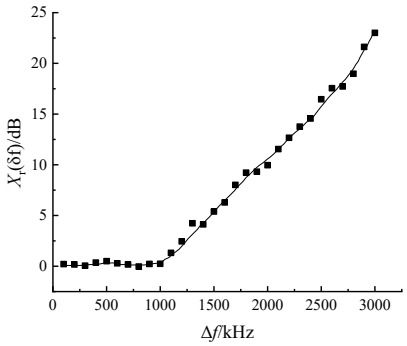

Fig. 8. The variation curve of $X_r(\delta f)$ with the interference frequency difference δf.

Δf_i [MHz]	0	20	40	60	80
$\gamma(\Delta f_i)$ [dB]	17.2	16.6	17.0	16.7	16.9
Δf_i [MHz]	100	120	140	160	165
$\gamma(\Delta f_i)$ [dB]	16.7	17.0	17.2	16.3	16.0
Δf_i [MHz]	170	175	180	200	220
$\gamma(\Delta f_i)$ [dB]	15.7	13.3	13.0	10.8	9.6

Tab. 6. The test result of $\gamma(\Delta f_i)$ of positive frequency bias.

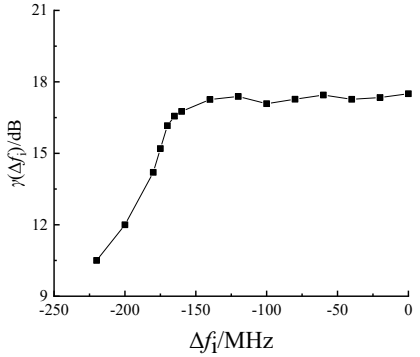

Fig. 9. Relationship between $\gamma(\Delta f_i)$ and negative Δf_i.

experimental results are consistent. The SIFA interference sensitive bandwidth is about ±200 MHz.

In summary, the SIFA of the selected sensitive level will appear in EUT in the range of ±200 MHz of dual-frequency interference frequency bias and 3000 kHz of interference frequency difference. The SIFA interference is obvious in the range of ±150 MHz interference frequency offset and 1000 kHz interference frequency difference. The SIFA interference cannot be ignored.

5. Model Validation

To verify the accuracy of the model, according to formula (8), the SIFA effect index RF is calculated from the interference frequency difference $\delta f = f_1 - f_2$ and the interference frequency offset $\Delta f_i = f_i - f_0$, calculate the SIFA effect index R_F to verify the accuracy of the effect model.

1) Change the intermodulation frequency difference δf. Set the $f_1 = 0$ kHz, f_2 changed, and calculated effect index is shown in Tab. 7.

2) Change the intermodulation frequency offset Δf_i. Combined with the test data in Tab. 2 and 3 in Sec. 4, the R_F test results under different frequency offsets are shown in Tab. 8.

It can be seen from Tab. 7 and Tab. 8 that the maximum test error of R_F of the SIFA effect model of the dual-frequency EMI of the EUT is less than 1 dB.

6. Conclusion

To meet the demand of radar SIFA interference test, the SIFA effect model is theoretically derived by introducing the SIFA action factor $\gamma(\Delta f_i)$ and the low-frequency false alarm relative level $X_r(\Delta f)$. Secondly, the SIFA effect model parameter testing method is proposed for radar, which is characterized by the fact that the radar's sensitive radiation frequency deviation is much larger than its sensitive intermodulation frequency difference. Subsequently, the accuracy of the effect assessment is verified by experiments. Based on the theoretical derivation and experimental testing of the SIFA interference effect, the evaluation

δf [kHz]	20	40	60	80
$\gamma(\Delta f_1)$ [dB]	20.8	20.9	21.1	20.9
$\gamma(\Delta f_2)$ [dB]	20.8	20.9	21.1	20.9
$X_r(\delta f)$ [dB]	0.5	0.4	0.0	0.3
R_F [dB]	0.7	0.2	0.0	–0.6

Tab. 7. Test results under different frequency deviations.

Δf_1 [kHz]	0	200	400
Δf_2 [kHz]	200	400	600
$\gamma_F(\Delta f_1)$ [dB]	19.8	19.5	19.7
$\gamma_F(\Delta f_2)$ [dB]	19.5	19.5	19.7
$X_r(\delta f)$ [dB]	0.3	0.3	0.7
R_F [dB]	0.3	–0.3	–0.7

Tab. 8. Test results under different frequency offsets.

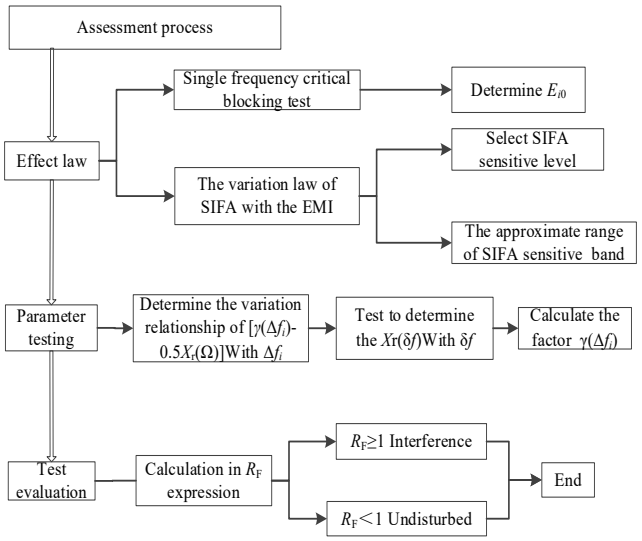

Fig. 10. Prediction process of SIFA interference effect.

process for SIFA interference of radar is presented as follows. In practical applications, it is possible to evaluate whether the equipment is affected by second-order intermodulation false alarm interference based on the single frequency electromagnetic blockage change curve of radar equipment and the environmental electromagnetic field spectrum distribution parameters, using an effect model.

Acknowledgments

This work was supported by the fund project of the Key Laboratory (No. 6142205200301) and key national defense basic research projects (No. 50909030201).

References

[1] WANG, L., SHEN, X., ZHOU, B. Review on cognition of complex electromagnetic environment. *Aerospace Electronic*

Warfare, 2020, vol. 36, no. 2, p. 1–6. DOI: 10.16328/j.htdz8511.2020.02.002

[2] DU, X., WEI, G., REN, S. Analysis of blocking effect for single frequency continuous wave electromagnetic radiation in swept frequency radar. *Chinese Journal of Systems Engineering and Electronics*, 2020, vol. 42 no. 12, p. 2742–2746. DOI: 10.3969/j.issn.1001-506X.2020.12.09

[3] TANG, Z. Y., YU, C. R., DENG, Y. K. Evaluation of deceptive jamming effect on SAR based on visual consistency. *IEEE Journal of Selected Topics in Applied Earth Observations and Remote Sensing*, 2022, vol. 11, p. 12246–12262. DOI: 10.1109/JSTARS.2021.3129494

[4] LIU, C., WU, R., HE, Z., et al. Modeling and analyzing interference signal in a complex electromagnetic environment. *EURASIP Journal on Wireless Communications and Networking*, 2016, vol. 4, no. 1, p. 1–9. DOI: 10.1186/s13638-015-0498-8

[5] KASHMOOLA, M., ANAD ALSALEEM, M. Y., ANAD ALSALEEM, N. Y., et al. Model of dynamics of the grouping states of radio electronic means in the problems of ensuring electromagnetic compatibility. *Eastern-European Journal of Enterprise Technologies*, 2019, vol. 6, no. 9, p. 12–20. DOI: 10.15587/1729-4061.2019.188976

[6] ZHAO, B., HUANG, L., ZHANG, J. Single channel SAR deception jamming suppression via dynamic aperture processing. *IEEE Sensors Journal*, 2017, vol. 17, no. 13, p. 4225–4230. DOI: 10.1109/JSEN.2017.2695001

[7] ANTIPIN, B. M., VINOGRADOV, E. M., TUMANOVA, E. I., et al. Estimation of intermodulation products in radio receivers of radiocommunication systems. In *Conference of Russian Young Researchers in Electrical and Electronic Engineering (ElConRus)*. Saint Petersburg (Russia), 2022, p. 16–18. DOI: 10.1109/ElConRus54750.2022.9755642

[8] ALASTALO, A. T., KAAJAKARI, V. Third-order intermodulation in microelectromechanical filters coupled with capacitive transducers. *IEEE Journal of Microelectromechanical Systems*, 2006, vol. 15, no. 1, p. 141–148. DOI: 10.1109/JMEMS.2005.863705

[9] RUPAKULA, B., REBEIZ, G. M. Third-order intermodulation effects and system sensitivity degradation in receive-mode 5G phased arrays in the presence of multiple interferers. *IEEE Transactions on Microwave Theory and Techniques*, 2018, vol. 66, no. 12, p. 5780–5795. DOI: 10.1109/TMTT.2018.2854194

[10] ALASTALO, A. T., KAAJAKARI, V. Intermodulation in capacitively coupled microelectromechanical filters. *IEEE Electron Device Letters*, 2005, vol. 26, p. 289–291. DOI: 10.1109/LED.2005.846589

[11] YANG, Y., KIM, B. A new linear amplifier using low-frequency second-order intermodulation component feedforwarding. *IEEE Microwave and Guided Wave Letters*, 1999, vol. 9, no. 10, p. 419 to 421. DOI: 10.1109/75.798035

[12] MANSTRETTA, D., BRANDOLINI, M., SVELTO, S. Second-order intermodulation mechanisms in CMOS downconverters. *IEEE Journal of Solid-State Circuits*, 2019, vol. 38, no. 3, p. 394 to 406. DOI: 10.1109/JSSC.2002.808310

[13] ZHAO, H. Z., WEI, G. H., DU, X., et al. Analysis of third-order intermodulation blocking effect for satellite navigation receiver (in Chinese). *Journal of Systems Engineering and Electronics*, 2020, vol. 44, no. 4, p. 1336–1342. DOI: 10.12305/j.issn.1001-506X.2022.04.32

[14] WANG, Y., WEI, G., LI, W., et al. Mechanism modeling and verification of receiver with in-band dual-frequency blocking jamming (in Chinese). *Transactions of Beijing Institute of Technology*, 2018, vol. 38, no. 7, p. 709–714. DOI: 10.15918/j.tbit1001-0645.2018.07.008

[15] ZHAO, H. Z., WEI, G. H., PAN, X. D., et al. Prediction method of multi-frequency non-intermodulation electromagnetic radiation blocking effect of BeiDou navigation receiver. *AIP Advances*, 2022, vol. 12, p. 1–9. DOI: 10.1063/5.0096545

[16] LI, W., WEI, G. H., PAN, X. D., et al. Electromagnetic compatibility prediction method under the in-band interference environment. *IEEE Transactions on Electromagnetic Compatibility*, 2018, vol. 6, no. 2, p. 520–528. DOI: 10.1109/TEMC.2017.2720961

[17] WEI, G., ZHENG, J. A model for predicting second-order intermodulation low-frequency blocking effects. *IEEE Transactions on Electromagnetic Compatibility*, 2022, vol. 64, no. 2, p. 348–357. DOI: 10.1109/TEMC.2021.3121392

[18] WEI, G., ZHENG, J., ZHAO, H., et al. Modeling and evaluation method of second-order intermodulation LF blocking effect for spectrum-dependent equipment (in Chinese). *Transaction of Beijing Institute of Technology*, 2021, vol. 41, no. 10, p. 1095–1102. DOI: 10.15918/j.tbit1001-0645.2020.224

[19] DU, X., WEI, G., ZHAO, K., et al. Research on dual-frequency electromagnetic false alarm interference effect of a typical radar. *Sensors*, 2022, vol. 22, p. 1–13. DOI: 10.3390/s22093574

[20] DU, X., WEI, G. Effect of continuous wave electromagnetic environment on radar equipment. *Journal of Army Engineering University of PLA*, 2022, vol. 1, no. 8, p. 36–42.

[21] DU, X., WEI, G., ZHAO, K., et al. Research on continuous wave electromagnetic effect in swept frequency radar. *Mathematical Problems in Engineering*, 2021, p. 1–10. DOI: 10.1155/2021/4862451

[22] EQUIPMENT DEVELOPMENT DEPARTMENT OF THE CENTRAL MILITARY COMMISSION. *GJB8848-2016. Electromagnetic Environmental Effects Test Methods for Systems.* Beijing, 2016.

[23] MILITARY STANDARD PRESS OF GENERAL EQUIPMENT DEPARTMENT. *GJB 151B-2013. Electromagnetic Emission and Susceptibility Requirements and Measurements for Military Equipment and Subsystems*. Beijing, 2013.

About the Authors …

Xue DU received the Ph.D. degree in Weapon Science and Technology from the Shijiazhuang Campus of the Army University of Engineering in 2023, China. She is currently a teaching assistant with the Artillery Engineering Department of the campus. Her research interests include testing methods for electromagnetic environmental effects and evaluating equipment interference effects.

Guanghui WEI received the B.Sc. and M.Sc. degrees in Physics from Nankai University, Tianjin, China, in 1984 and 1987, respectively. He is currently a Professor with the National Key Laboratory of Electromagnetic Environment Effects, Shijiazhuang, China. His research interests include reverberation chambers, computational electromagnetic, EMC test environments and EMC measurement techniques.

Dalin WU received the Ph.D. degree in Weapon Science and Technology from the Shijiazhuang Campus of the Army University of Engineering in 2017. He is a lecturer with the Artillery Engineering Department of the campus. His research interests include weapon structural dynamics and simulation, vehicle engineering, and artillery systems.

Xiaodong PAN received the Ph.D. degree in Electromagnetic Compatibility and Protection from the Mechanical Engineering College, China, in 2014. He is currently an Associate Professor in the National Key Laboratory of Electromagnetic Environment Effects, Army Engineering University, Shijiazhuang Campus. His research interests include EMC test environments and EMC measurement techniques.